Chemical Engineering Journal 507 (2025) 159897

Contents lists available at ScienceDirect

Chemical Engineering Journal

journal homepage: www.elsevier.com/locate/cej

Machine learning-based prediction and optimization of plasma-catalytic dry reforming of methane in a dielectric barrier discharge reactor

Jiayin Li [a,*], Jing Xu [b], Evgeny Rebrov [c,d], Annemie Bogaerts [a,*]

[a] Research Group PLASMANT, University of Antwerp, Department of Chemistry, Antwerp 2610, Belgium
[b] School of Electronic Information and Communications, Huazhong University of Science and Technology, Wuhan, Hubei 430074, People's Republic of China
[c] School of Engineering, University of Warwick, Coventry CV4 7AL, the United Kingdom
[d] Department of Chemical Engineering and Chemistry, Eindhoven University of Technology, P.O. Box 513, 5600 MB Eindhoven, the Netherlands

ARTICLE INFO

Keywords:
Plasma catalysis
Dry reforming of methane
Machine learning
Process optimization
Syngas production

ABSTRACT

We developed an innovative machine learning (ML) model, including a supervised learning (SL) and reinforcement learning (RL) model, to predict and optimize the plasma-catalytic dry reformation of methane (DRM) over Ni/Al_2O_3 catalysts in a dielectric barrier discharge (DBD) reactor based upon experimental data. To tackle its intricate and non-linear characteristics, the SL model uses artificial neural networks (ANN) to accurately predict the performance, achieving excellent consistency with the experimental results. The RL model subsequently investigates the optimal optimization policy, namely starting with a coarse tuning of the more influential parameters, followed by fine-tuning of the less important parameters, to obtain the best performance. The optimal results show that a discharge power at lowest bond (i.e., 20 W) but CO_2/CH_4 ratio at highest bond (i.e., 1.5) result in the minimum energy cost (21 eV/molec), validated by our SL model and experimental data. Furthermore, we also investigated the simultaneous optimization of total conversion and energy cost, resulting in a maximum total conversion of 36 %, combined with a minimum energy cost of 34 eV/molec, at a Ni loading of 9.5 wt%, discharge power of 60 W, and total flow rate of 74 mL/min. Our ML model showcases an impressive capacity to derive advantageous insights from existing datasets, thereby advancing and optimizing plasma-catalytic chemical processes.

1. Introduction

Carbon dioxide (CO_2) and methane (CH_4) are the two major greenhouse gasses that significantly contribute to climate change [1]. Currently, there is an urgent need for their conversion into value-added chemicals [2,3]. Dry reforming of methane (DRM) presents an emerging method for the concurrent conversion of both CO_2 and CH_4, yielding valuable syngas (i.e., CO and H_2), as shown in Eq. (1). The syngas can serve as a hydrogen source or to further process to produce higher-value chemicals, e.g., methanol and formaldehyde [4,5].

$$CH_4 + CO_2 \rightarrow 2CO + 2H_2, \Delta H_0 = 247.3\,kJ/mol \quad (1)$$

Non-thermal plasma (NTP), a cutting-edge technology, enables this reaction operating at mild temperatures and ambient pressure [6–8], providing a valuable approach to traditional methods. Indeed, a recent techno-economic analysis, applied to a pilot plant producing 100 tCO/day, revealed that the energy cost of plasma-based CO_2 conversion is 43 % less than for electrolysis and conventional CO_2 conversion methods, and that using a post-plasma carbon bed is crucial for this cost-effectiveness, to facilitate additional CO production from O_2 and enhancing the CO_2 conversion [9].

Plasma is a partially (or fully) ionized gas, containing charged species, radicals and exited species that exhibit collective behavior. The presence of radicals and highly energetic electrons enables reaction pathways that would otherwise be impossible, making plasma reactors valuable for converting thermodynamically stable molecules like CO_2 and CH_4. The catalyst can further promote the selective syngas production, while combining it with plasma holds significant promise for generating a synergistic effect that boosts overall efficiency, although synergy is not always reached and more insight is needed in the underlying mechanisms [10,11]. Furthermore, plasma is generated with electricity, and can be rapidly switched on and off, thus facilitating its integration with the fluctuating nature of renewable energy sources [12].

* Corresponding authors.
E-mail addresses: jiayin.li@uantwerpen.be (J. Li), annemie.bogaerts@uantwerpen.be (A. Bogaerts).

https://doi.org/10.1016/j.cej.2025.159897
Received 17 September 2024; Received in revised form 17 December 2024; Accepted 22 January 2025
Available online 30 January 2025

Over the past few decades, a wide range of plasma reactors have been thoroughly tested for plasma-based DRM applications, such as glow discharge [13], corona discharge [14], gliding arc [15], microwave discharge (MW) [16] and dielectric barrier discharge (DBD) [17–20]. Because of its simple design and user-friendly nature, especially when combined with packing materials, most plasma catalysis research so far has utilized DBDs, within a coaxial reactor [7]. In general, the reaction performance and cost-effectiveness of plasma reactors are considered for evaluation, both of which are very important. Although the total conversion for DBD reactors can be quite high, the energy cost is often excessively high [21,22]. On the other hand, it is complicated to select for optimal performance as the input parameters also requires balancing chemical performance and cost-effectiveness [7]. Therefore, combining high conversions with relatively low energy costs is really challenging due to the many interacting parameters in complex plasma-catalytic systems [10,11].

To address these challenges, machine learning (ML) methods offer a novel pathway for exploring intricate scientific phenomena, and they are receiving growing attention for plasma processes, such as in plasma medicine [23–25], for the synthesis of chemicals [26,27] and in pollution control [28]. In general, ML methods can be broadly divided into two categories: (a) supervised learning (SL), which uses both input (predictors) and output (predicted variables) data, to effectively learn a mapping between them, but it requires large amounts of data; and (b) unsupervised learning, which relies solely on input data to learn patterns or correlations for finding hidden patterns or structures in input data, but the results are often harder to interpret and validate. In plasma catalysis, previous studies have primarily utilized SL (referred to as ML in many papers) models, typically by artificial neural network (ANN) algorism, for chemical performance prediction. For example, Liu et al. [29] successfully predicted the reaction performance in plasma-based CH_4 conversion to hydrocarbons. Similarly, Zhu et al. [30] elucidated the relationships between operation parameters and performance of CH_3OH oxidation. Wang et al. [31] revealed that both higher gas conversion and energy efficiencies were favor at optimal conditions of 10–20 W and 5–20 °C. Recently, Cai et al. [32] found the optimal condition led to the maximum energy yield in plasma-catalytic DRM by a hybrid SL model. Despite the promise of ML in catalysis, the optimization of plasma-catalytic DRM by ML is however still in its infancy.

The complex plasma–catalyst interactions can be divided into two categories: the effects of plasma on the catalyst, and the effects of the catalyst on the plasma. Hence, changing one of the effects may have unpredictable influence on the other effects. In addition, the optimization process for the operating conditions likely leads to trade-offs among conflicting objectives (e.g., higher conversion and product yields, or higher energy efficiency), and the SL approach is not always accurate and robust enough for solving such multi-target problems. To achieve a cost-effective plasma-catalytic system with good reaction performance, it is crucial to obtain a thorough understanding on how the interconnected operating parameters can be optimized [13]. However, no studies consider the optimization of both total conversion and energy cost in plasma-catalytic DRM. Considering traditional trial-and-error efforts in experiments have reached their limit, and the simultaneous multi-objectives optimization, based on many interacting parameters, is challenging.

Reinforcement learning (RL), another major subset of ML, is a goal-direct approach, which involves how to maximize the outcome by mapping actions, to steer future experimental work [33]. The RL agents can learn to achieve specific goals by actively interacting with the environment, bypassing the necessity to a priori develop an accurate mathematical physico-chemical model [34]. This approach leverages RL's two strengths – obtaining performance via experience and preventing reliance on exact models, are especially beneficial for complex plasma-surface reactions, where it is not yet feasible to construct a precise dynamic model based on first principles, and the dynamic characteristics are highly variable [35]. However, the quality and quantity of training dataset matter most in the performance of RL models. In previous work, Cai et al., [32], carried out a comprehensive investigation, involving 100 distinct reaction conditions, to ensure the robustness and relevance for further RL model development.

In this work, we designed a very first RL model to simultaneously maximize the total conversion and minimize the energy cost in plasma-catalytic DRM, in an attempt to develop an artificial intelligence (AI) method for plasma catalysis. Firstly, we developed the prediction model for reaction performance (CO_2 and CH_4 conversion, H_2 and CO yield, total conversion) and cost-effectiveness (energy cost) by the ANN algorithm. Subsequently, we designed RL controllers (agents) by using the prediction model as simulation environment for learning interactions. Finally, the output from the RL model is compared with the actions chosen from four operating parameters, including Ni loading, total gas flow rate, CO_2/CH_4 ratio and discharge power. Therefore, by mapping these operating parameters, the RL model can determine the fine-tuning steps that achieve cost-effectiveness as well as good reaction performance in plasma-catalytic DRM.

2. Methodology

In this work, we used two ML methods, i.e., SL and RL, to develop the model describing the plasma-catalytic DRM process, as schematically illustrated in Fig. 1, and detailly elaborated in the subsequent sections.

2.1. Data collection and processing

Fig. S1 shows the experimental setup for DRM, which is detailly described in Ref. [20]. The total conversion χ_{total} is of great importance, and obviously more complicated for optimization, which is defined by the summing of the effective CO_2 and CH_4 conversions [36]:

$$\chi_{total} = \sum_i \chi_i^{eff} = \chi_{CO_2}^{abs} \cdot y_{CO_2}^{in} + \chi_{CH_4}^{abs} \cdot y_{CH_4}^{in} \quad (2)$$

where the absolute CO_2 conversion $\chi_{CO_2}^{abs}$ times the inlet CO_2 fraction $y_{CO_2}^{in}$ and the absolute CH_4 conversion $\chi_{CH_4}^{abs}$ times the inlet CH_4 fraction $y_{CH_4}^{in}$. The energy cost (EC in unit eV/molec) is defined as [7]:

$$EC(eV/molec) = \frac{SEI(eV/molec)}{\chi_{total}} = \frac{Power\,(kW)\cdot 60s/\min\cdot\left(24.05\,L/mol * 6.24 * 10^{21} eV/kJ\right)}{Total\,gas\,flow\,rate\,(L/\min)\cdot\chi_{total}\cdot 6.02 * 10^{23}\,molec/mol} \quad (3)$$

By varying the above-mentioned process parameters, the actual reaction performance and EC were collected as the dataset, which can be found in the Supplementary Material (Table S2, S3). Before model development, all datasets were pre-process by a Min-Max normalization method [37]. The normalized data is confined to the same interval, which accelerates the convergence of the network and avoids the saturation of neurons, as shown in Eq. S1 and Eq. S2 in Supplementary Information (SI). The complete dataset was divided into 70 % training subset and 30 % testing subset. If the ratio between training and test set would be reduced, the ML prediction capability and quality will be lower, as less data will be used for training and more data will be used for testing. The ML model may fail to learn the underlying structure of the data, leading to underfitting and poor generalization ability. Also, if the ratio would be increased, the ML prediction capability and quality will be also lower. Although more data is used for training to identify learning patterns, there will be less test data, which may affect the reliability and stability of the evaluation results, as a smaller test set may not fully represent the diversity of the overall dataset.

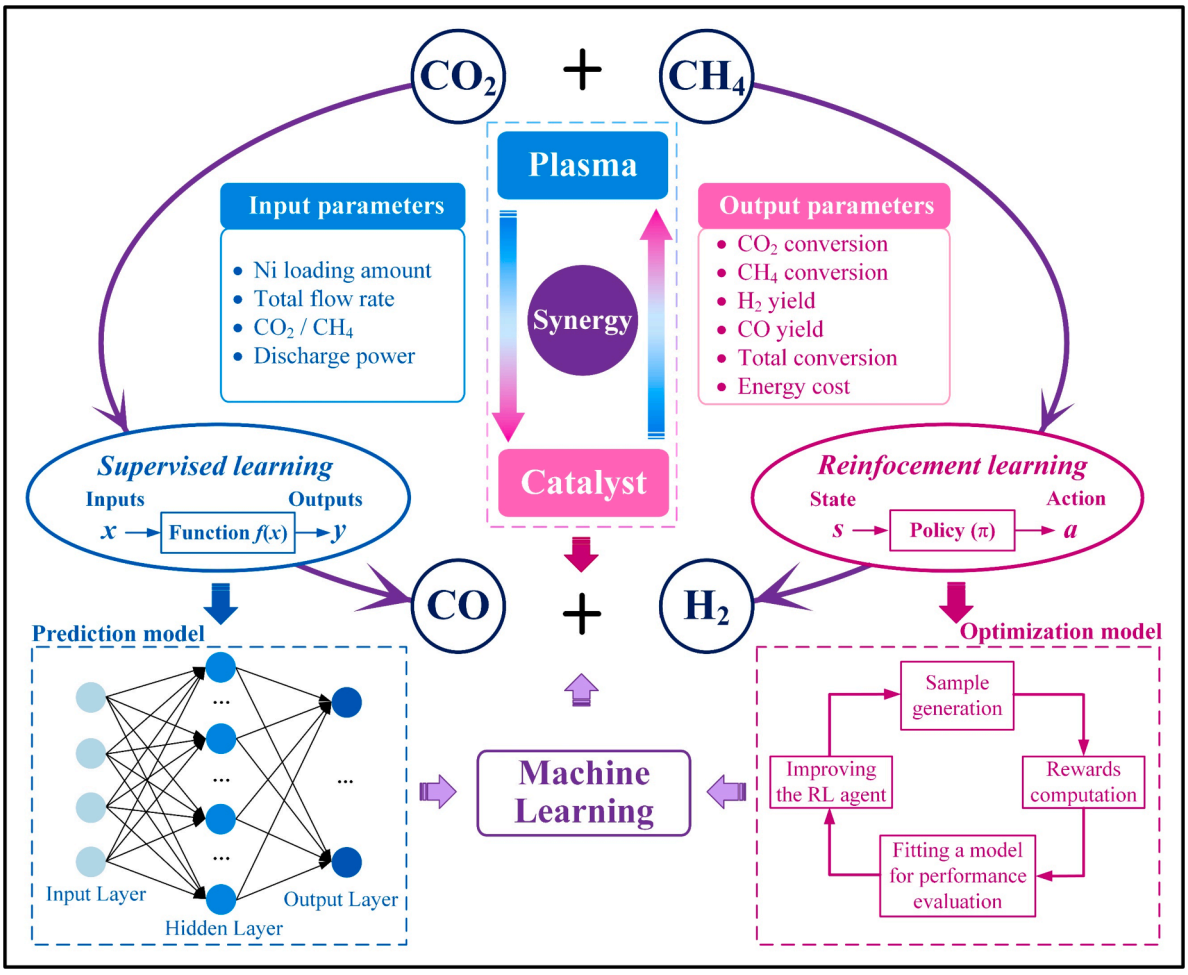

Fig. 1. Overview of the ML model for plasma-catalytic DRM. A SL model predicts the output variable y by mapping input variables x through a function $f(x)$; A RL optimization model involves how to map states to actions based on policy (π).

2.2. Description of the artificial neural network

The artificial neural network (ANN), a conventional SL algorithm, was utilized to estimate the performance of plasma-based DRM under various operating conditions, as it exhibits remarkable predictive accuracy to solve the nonlinear problems. The network contains numerous artificial neurons inside, with connection weights between them, serving as learnable parameters. Typically, an ANN model comprises multiple layers, each of which consists of numerous nodes. Each node corresponds to one dimension of input and output data. In this work, each layer is fully connected to the previous and subsequent layers. The four above-mentioned operating parameters are used as inputs, while six above-mentioned performances are selected as the targets for prediction.

We used the backpropagation (BP) algorithm to optimize the network parameters by gradient descent [38]. To address the nonlinear problem and mitigate the gradient disappearance issue, we used the tanh function as the model's activation function. To enhance the gradient descent algorithm's efficiency, we used the mean square error (MSE) as loss function, which ensures faster convergence and performs well in solving regression tasks. Meanwhile, MSE and coefficient of determination (R^2) as evaluation metrics to measure the performance of the ANN model, respectively [39]:

$$MSE = \frac{1}{n}\sum_{i=1}^{n}(y_i - \hat{y}_i)^2 \tag{4}$$

$$R^2 = 1 - \frac{\sum_{i=1}^{n}(y_i - \hat{y}_i)^2}{\sum_{i=1}^{n}(y_i - \bar{y})^2} \tag{5}$$

where y_i denotes the actual value, $\hat{y}_i$ denotes the predicted value and $\bar{y}$ indicates the average of the actual value. Generally, higher R^2 and lower MSE are desirable to enhance the model accuracy [40]. Furthermore, we employed the grid search method to fine-tune the hyperparameters for the ANN algorithm, as it effectively processes intricate models with multiple parameters [41]. After the optimization (see MSE plotted in Fig. S2), we listed the parameters of the ANN model in Table 1.

2.3. Methods of significance analysis

The Pearson's Correlation Coefficient (PCC) was utilized to access

Table 1
Detailed parameters of the ANN model.

Parameter	ANN model
Number of input layers	4
Number of hidden layer 1	15
Number of hidden layer 2	10
Number of output layers	4
Activation function	tanh
Optimizer	lbfgs
Loss function	MSE
Evaluation indicator	MSE and R^2

the linear dependency between different input variables, which is given by [42,43]:

$$\rho_{xy} = \frac{\sum (x_i - x_{mean})(y_i - y_{mean})}{\sqrt{\sum (x_i - x_{mean})^2 \sum (y_i - y_{mean})^2}} \quad (6)$$

where ρ_{xy} represents PCC value between the input feature and output target ranging from −1 (negative) to +1 (positive). The x_{mean} denote the averages of input feature x and y_{mean} denotes the averages of output target y. According to the absolute values of the PCC, we can evaluate the relative importance of four operating parameter for all reactor performance, as shown in Fig. S3.

2.4. Description of the RL model

SL models are designed to predict patterns, but they do not involve decision-making process. In contrast, RL models develops the optimal decision policy by interacting with the environment [34]. Since the RL system's actions will impact its future inputs, it can be treated as a feedback control system based on rewards. The learner, so-called agents developed by RL, is not guided on specific actions, rather it must explore which actions maximize the rewards. A reward signal determines the goal in an RL problem, which is affected by the agent's current action and the current state of the environment, and in turn, the agent can directly influence on reward, or indirectly influence through changing the environment's state. Accordingly, a policy is used to guide the agent on the appropriate action to take in those states, to maximize the return (the expected accumulated discounted reward over the course of an episode). It is the job of the algorithm to automatically figure out how to choose good actions.

As shown in Fig. 1, RL typically involves four essential steps to train an agent. More details on the RL agent are described in Fig. S4. Our goal is to design such RL agents that determine the four above-mentioned operating parameters to explore the maximum reaction performance and minimum EC both within and outside the investigated range. In this work, the agent was trained by the Proximal Policy Optimization (PPO) algorithm built on the Actor-Critic (AC) framework (see Fig. S5 and S6 in SI), which has good performance within the continuous data space [44]. By observing the agent's behavior, one can conclude the optimal policy of reaction performance and cost-effectiveness based on its decision process. The detailed parameters of the RL model are listed in Table S4.

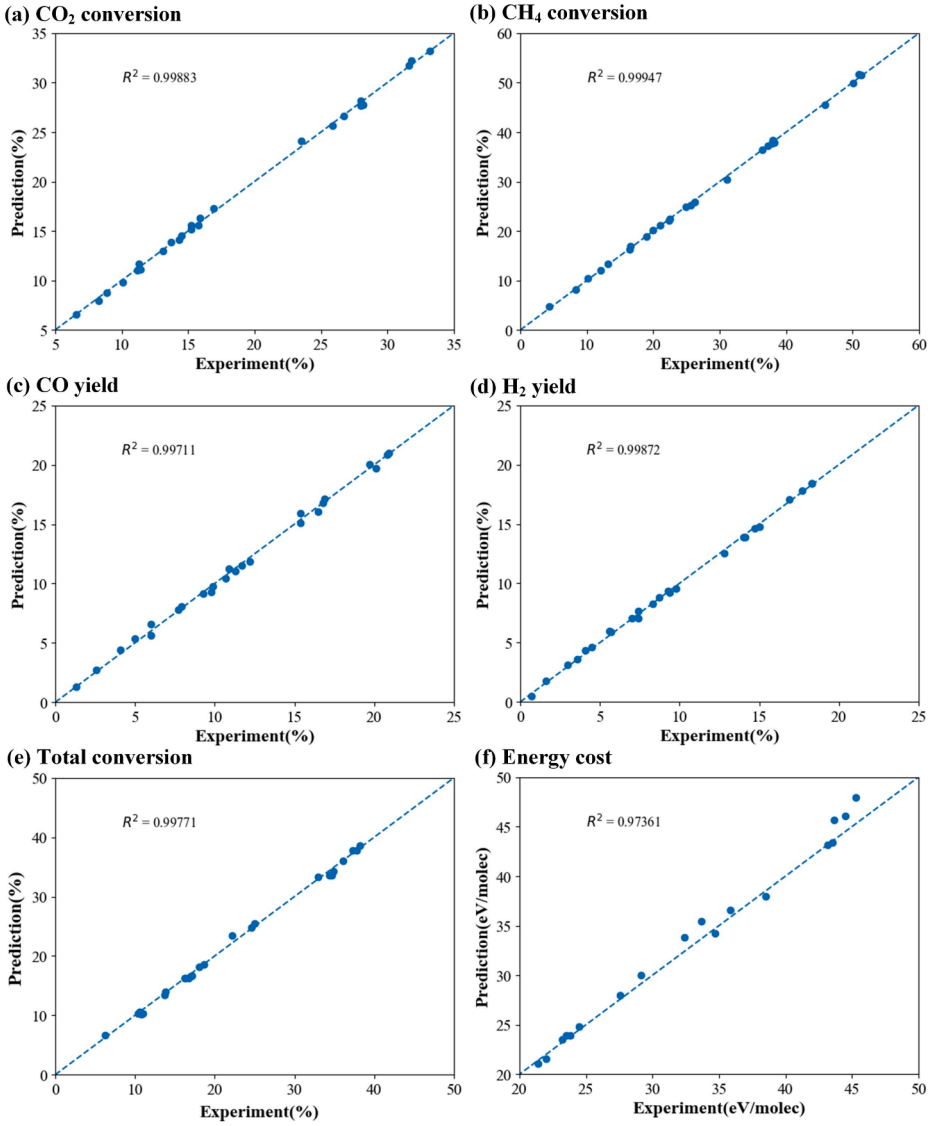

Fig. 2. Predicted data versus experimental results (R^2 plot). (a) CO_2 conversion; (b) CH_4 conversion; (c) CO yield; (d) H_2 yield; (e) total conversion and (f) energy cost.

3. Results

3.1. ANN model evaluation

We assess the ANN model's performance by comparing its prediction values and actual values for reaction performance and cost-effectiveness, as shown in Fig. 2 and Fig. S7. This ANN prediction model exhibits impressive accuracy through the complete dataset, achieving an R^2 consistently near 1 and an MSE of only 0.000026. This highlights the ANN model has exceptional ability in forecasting the plasma-catalytic DRM process, providing a robust basis for developing the RL model. To further evaluate the model's generalizability, we conducted additional experiments using new operating parameters within the investigated ranges. As presented in Fig. S8, the model's predictions on unseen data aligned well with the actual data, thereby confirming its reliability.

3.2. Significance and trend analysis of parameters

The relative significance of each factor and the trend between input operating parameters and output performance parameters are demonstrated in Table 2. The most important factor is total flow rate for CO_2 conversion (56.6 %), CH_4 conversion (43.5 %), CO yield (49.5 %) and H_2 yield (51.0 %), as well as for total conversion (57.3 %). Additionally, the discharge power has a considerable positive influence (>20 %) on all these reaction performances. For the EC, the relative significance of total flow rate (43.1 %) and discharge power (39.1 %) are very close to each other. The CO_2/CH_4 ratio and discharge power exerts similar influences on gas conversion and product yield. It should be noted that Ni loading has minimal influence on overall process performance indicators (less than 7 %), indicating that the plasma characteristic plays a more critical role.

3.3. RL model evaluation

The investigated range of the four input parameters is as follows: Ni loading (5–15 wt%), CO_2/CH_4 ratio (0.5–1.5), discharge power (20–60 W) and total flow rate (25–125 mL/min). It would be interesting to first discover the theoretically (or potentially) maximum performance RL agents could reach without any physical limitation of input parameters (i.e. outside the investigated range). We will now establish the RL models, based on input parameters first outside and then within the investigated range.

Table 2
Relative significance of different input parameters on various output parameters.

Output Parameter	1st IF	2nd IF	3rd IF	4th IF
CO_2 conversion	Flow (56.6 %) (−)	Power (22.8 %) (+)	Ratio (17.2 %) (−)	Loading (3.3 %) (↗↘)
CH_4 conversion	Flow (43.5 %) (−)	Ratio (26.6 %) (+)	Power (23.5 %) (+)	Loading (6.4 %) (↗↘)
CO yield	Flow (49.5 %) (−)	Ratio (25.6 %) (+)	Power (21.0 %) (+)	Loading (3.9 %) (↗↘)
H_2 yield	Flow (51.0 %) (−)	Ratio (23.5 %) (+)	Power (21.6 %) (+)	Loading (3.8 %) (↗↘)
Total conversion	Flow (57.3 %) (−)	Power (27.9 %) (+)	Ratio (9.1 %) (↗↘)	Loading (5.8 %) (↗↘)
Energy cost	Flow (43.1 %) (↘↗)	Power (39.1 %) (+)	Ratio (14.6 %) (−)	Loading (3.2 %) (↘↗)

List of the abbreviations included in the table: Important factor (IF), Total flow rate (Flow), Discharge power (Power) and CO_2 /CH_4 ratio (Ratio). Positive factor and negative factor are represented by (+) and (−), respectively. Some output parameters first increased and then decreased with rising input parameters, indicated as (↗↘), while other output parameters first decreased and then increased with rising parameter, indicated as (↘↗).

3.3.1. Input parameters outside the investigated range

Fig. 3 shows the testing curve of the RL models of total conversion and EC with its corresponding actions, respectively. The total conversion (Fig. 3(a) and (b)) can reach a maximum of 55 %, while the agent first optimized the total flow rate until it converges to a negative value. Next, the agent optimized the discharge power, followed by the CO_2/CH_4 ratio, which converge to positive values. The Ni loading parameter also converges at a negative value, but it has low impact (<7 %) on the outputs compared with the other input parameters. Fig. 3 (c) shows that the minimum value of EC can reach almost 12 eV/molec, while the agent first optimized the discharge power to converge at a negative value, followed by the CO_2/CH_4 ratio. Fig. 3(d) shows the Ni loading and total flow rate already had their optimal value (i.e., not converged to the boundary of the operating range), while the CO_2/CH_4 ratio reached 1.9, which exceeds the current operating range (0.5–1.5). We notice that the actions on Ni loading and total flow rate are in line with the trend on EC shown in Table 2. Their trends are first decreasing and then increasing,

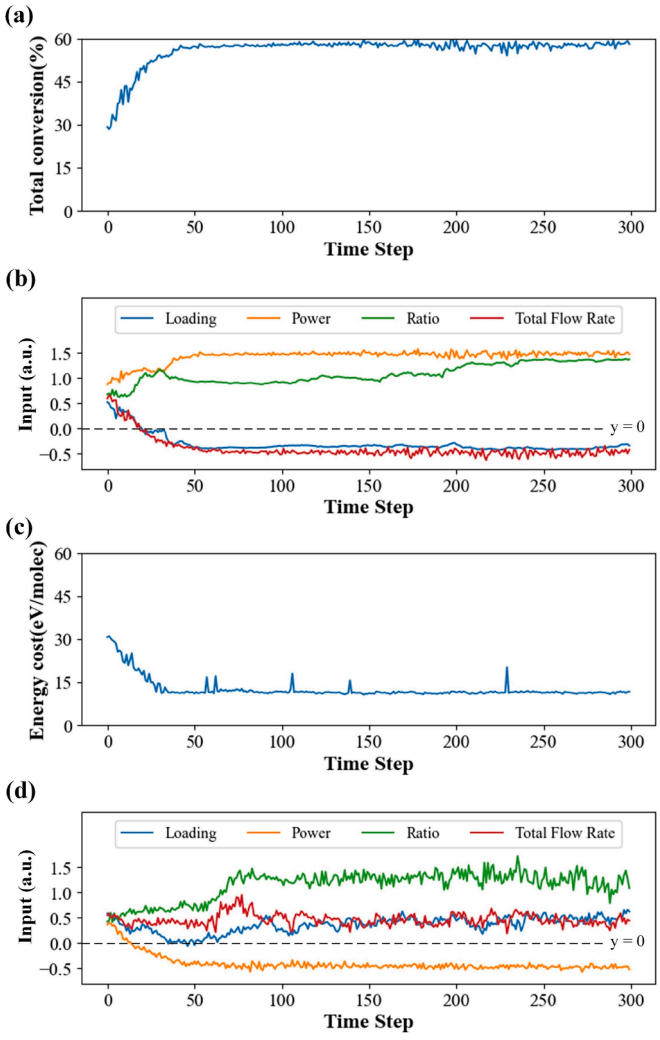

Fig. 3. Testing curve of the RL models of (a) total conversion and (c) energy cost, by plotting them as a function of time step, as well as the corresponding actions (b) and (d), outside the investigated range. The y-axis representing the input parameters (for (b) and (d)) shows the normalized values.

so the actions of the agent fluctuated to find its optimal value. Since the EC decreases with increasing CO_2/CH_4 ratio, the action on CO_2/CH_4 ratio increases and even exceeds the current operating range to obtain the minimum EC. It should be noted that the actions of total flow rate for the total conversion and of discharge power for the EC are not physical, as their value should be higher than 0 in reality.

We can also see that the discharge power converges to positive and negative values for total conversion and EC, respectively. Even though the input parameters are not restricted within their boundary, the positively and negatively correlated parameters reach their boundary value, as the dataset in the training process has upper and lower bounds as the time step progresses.

In real application of plasma-catalytic DRM, both total conversion and EC should be considered, and they are often affected in different ways by the input parameters (cf. also Table 2 above), so the best trade-offs should be determined. We simulate three cases, setting different weights between total conversion and EC, i.e., 1 (total conversion and EC are equally important), 2 (total conversion is twice as important), and 0.5 (EC is twice as important). The weighted superposition of total conversion and EC with its corresponding actions is shown in Fig. 4. The CO_2/CH_4 ratio is still proportional to the weighted superposition of total conversion and EC, since it monotonically converges to a positive value, even changing the weight (Fig. 4(b), (d) and (f)). A similar pattern can also be seen for the discharge power in Fig. 4(b) and (d). However, when the weight is 0.5, the power shows inverse effect on the weighted superposition of total conversion and EC. Moreover, the actions of flow rate and Ni loading present little difference, which means changing the flow rate and Ni loading is not effective for both total conversion and EC optimization.

3.3.2. *Input parameters within the investigated range*

To avoid the actions of agents reaching non-physical conditions, we now limit the input parameters within the investigated range of the training dataset (the reason will be further discussed in section 4.1). Fig. 5 shows the testing curve of the RL models of CO_2 conversion and CH_4 conversion, including their corresponding actions within the range of input parameters. Fig. 5(a) and (b) present that the CO_2 conversion can reach its maximum value of 42 % when the total flow rate first reaches its lower boundary (i.e. 25 mL/min), and then the discharge power reaches its upper boundary (i.e. 60 W), followed by the CO_2/CH_4 ratio reaching its lower boundary (i.e. 0.5). Nevertheless, the CH_4 conversion can reach its maximum value of 68 % when the total flow rate first reaches its lower boundary (i.e. 25 mL/min), followed by the CO_2/CH_4 ratio and discharge power reaching their upper boundary (i.e. 1.5 and 60 W). Furthermore, the actions of discharge power coincide very closely with the trajectory of CO_2 conversion and CH_4 conversion, indicating a fine-tuning step. As shown from the relative significance in Table 2, the most significant factor is the total flow rate for gas conversion, so the agent first optimized the total flow rate. While the discharge power is the second important factor for the CO_2 conversion, the agent optimized it as the second parameter. Moreover, the Ni loading keeps fluctuating within its range to seek its optimal value for both the CO_2 and CH_4 conversion, in line with the trend in Table 2 above, because of its low impact.

A similar regulation policy can be found in Fig. 6, which presents the time step-dependence of the CO yield and H_2 yield, with the corresponding actions, within the range of input parameters. Fig. 6(a) and (c) show that the CO yield can reach its maximum value of 28 % and the H_2 yield can reach its maximum value of 26 % when the total flow rate first reaches its lower boundary (i.e. 25 mL/min), followed by the CO_2/CH_4 ratio and the discharge power reaching their upper boundary (i.e. 1.5 and 60 W) (Fig. 6(b) and Fig. 6(d)), respectively. On the other hand, the Ni loading keeps fluctuating within its range to seek its optimal value for both the CO and H_2 yield, in line with the trend in Table 2 above, again because of its low impact.

The testing curve of the RL models for the total conversion and EC, with the corresponding actions within the investigated range, is presented in Fig. 7. From Fig. 7(a) and (b), we can see that the total conversion can reach its maximum value of 47 % when the total flow rate first reaches its lower boundary (i.e. 25 mL/min), followed by the discharge power reaching its upper boundary (i.e. 60 W), while the Ni

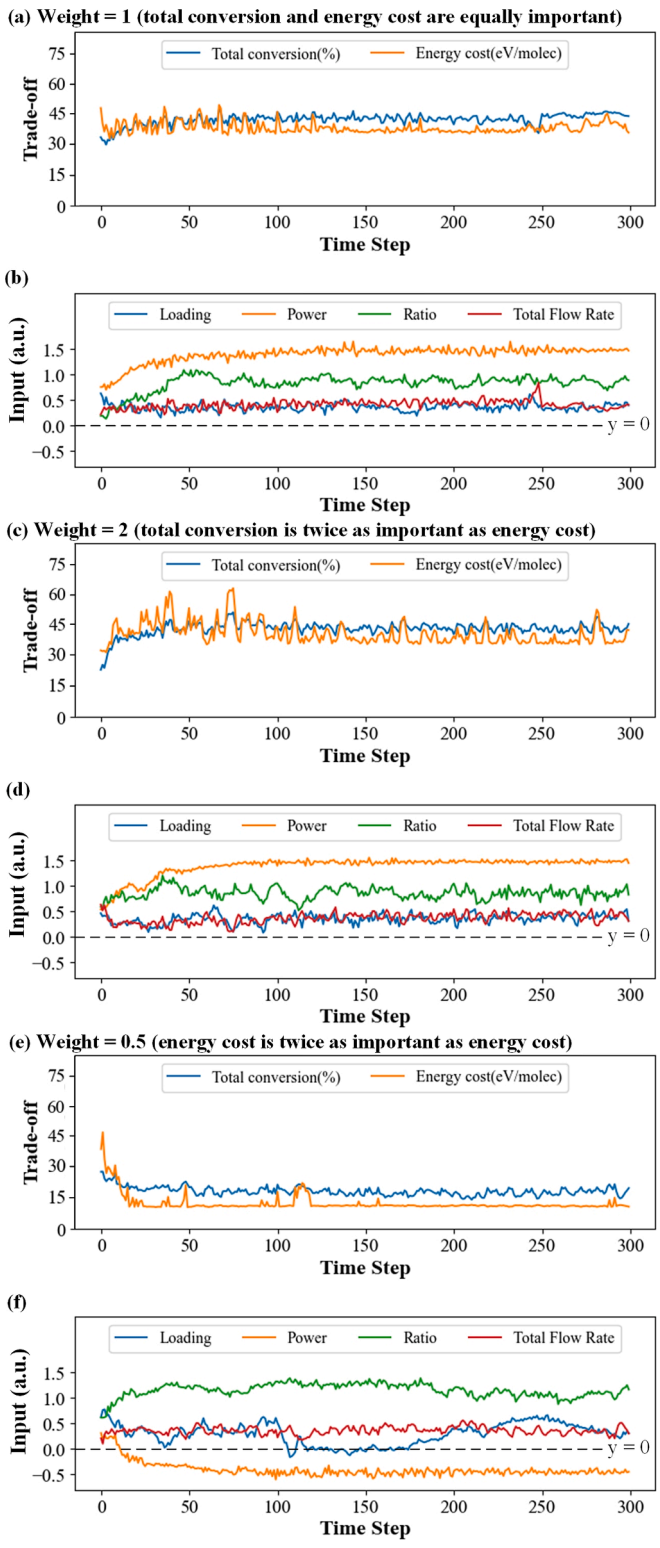

Fig. 4. Superposition of total conversion and energy cost, showing the best trade-offs (a,c,e), as well as the corresponding actions of the four input parameters outside the investigated range (b,d,f), for different weights, i.e., weight = 1: (a) and (b), weight = 2: (c) and (d), weight = 0.5: (e) and (f).

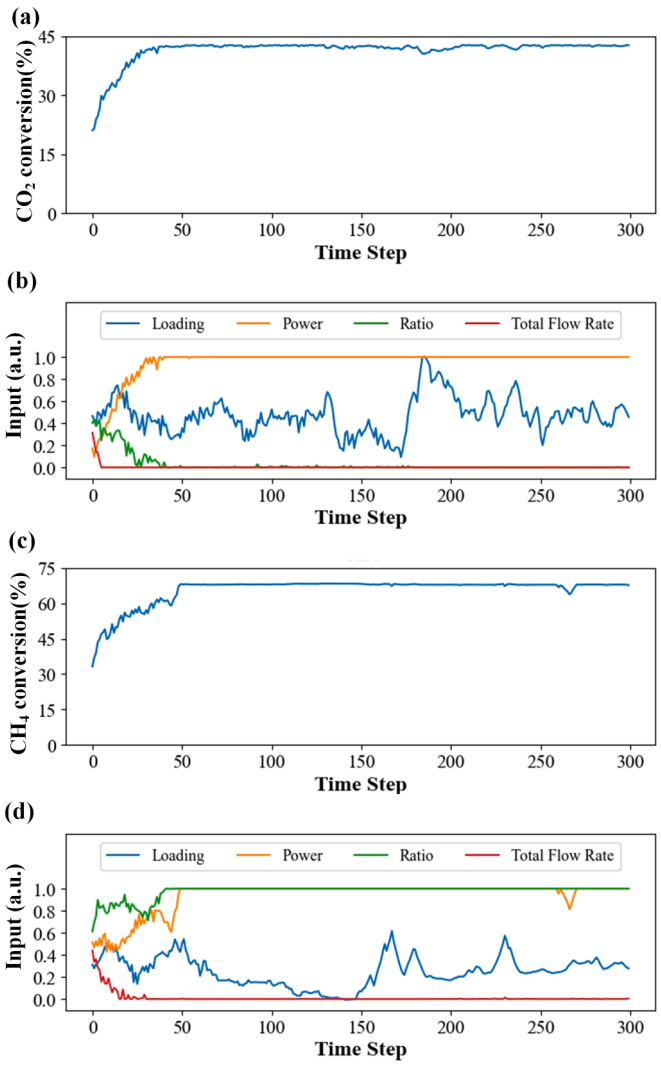

Fig. 5. Testing curve of the RL models of (a) CO_2 conversion and (c) CH_4 conversion, by plotting them against time step, as well as the corresponding actions (b) and (d), within the investigated range. The y-axis representing the input parameters (for (b) and (d)) shows the normalized values.

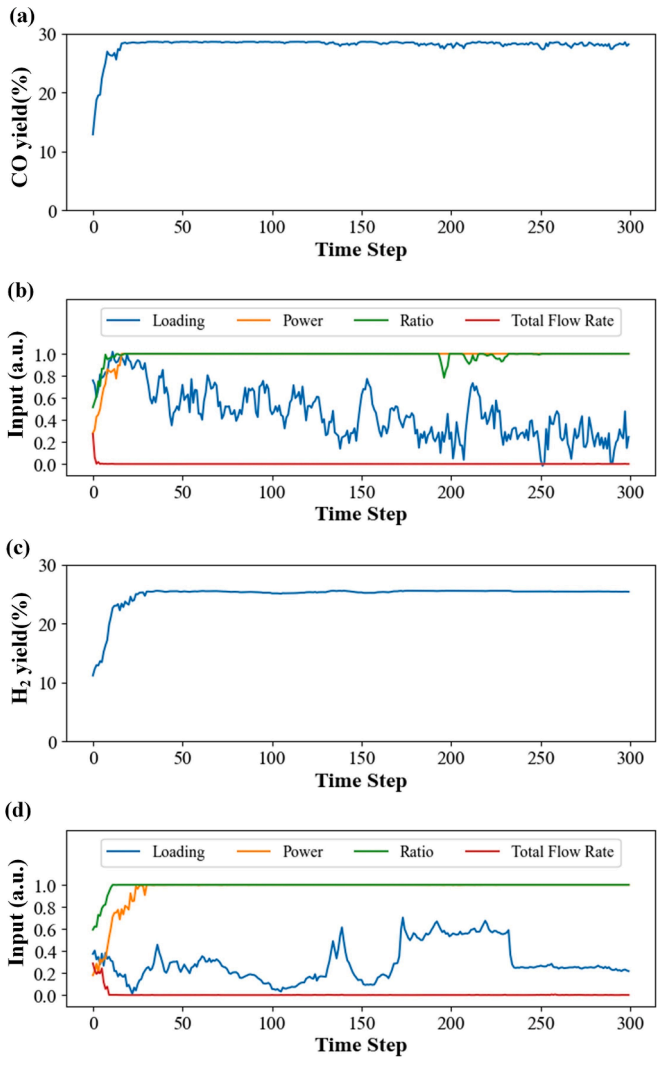

Fig. 6. Testing curve of the RL models of (a) CO yield and (c) H_2 yield, by plotting them as a function of time step, as well as the corresponding actions (b) and (d), within the investigated range. The y-axis representing the input parameters (for (b) and (d)) shows the normalized values.

loading and CO_2/CH_4 ratio have their optimal value at around 7.5 wt% and 1.3, respectively. The EC can reach its minimum value of 21 eV/molec when the power first reaches its lower boundary (i.e. 20 W), followed by the CO_2/CH_4 ratio reaching its upper boundary (i.e. 1.5). It is worth to point out that the discharge power yields a trade-off between total conversion and EC. Notably, eq. (3) suggests there is an inversely linear dependence between the total flow rate and the EC, but the total flow rate does not reach the upper boundary. The reason will be further clarified in Section 4.2.

In addition to separately investigating the total conversion and EC, we need a comprehensive understanding of the effect of all operating parameters for optimizing both performance metrics of the plasma-catalytic DRM process. Similar as in Section 3.3.1, we present in Fig. 8 the superposition of total conversion and EC for different weights, with the corresponding actions. When the total conversion is more or equally important than the EC, the discharge power is a positive factor and is near-linearly proportional to the weighted superposition. Especially when the total conversion is equally important to the EC, the total conversion reaches 36 %, while the EC reaches 34 eV/molec, when the discharge power reaches its upper boundary (i.e. 60 W), the Ni loading is 9.5 % and total flow rate is 74 mL/min. When the EC is more important than the total conversion, the power is a negative factor and is near-linearly but inversely proportional to the weighted superposition. Furthermore, the CO_2/CH_4 ratio has a positive correlation with the weighted superposition and fluctuates within the range to seek its optimal value, while the total flow rate and Ni loading seems at their fixed value.

4. Discussion

4.1. Effect of investigated range on the RL model

The investigated range of the training dataset has a noticeable effect on the RL model's performance. By comparing the two RL models of total conversion and energy cost outside and within the range in Fig. 3 and Fig. 7 (b and d), the total flow rate and discharge power converge to negative values and reach their lower boundary for total conversion and energy cost, respectively. We notice that the actions of agents reach negative values (i.e., −50 mL/min of total flow rate and −20 W of power), which is not in line with scientific knowledge, and impossible to implement as their value should be higher than 0 in reality. This phenomenon can be explained as follows: the total flow rate and discharge power are the negative factors and exhibit a near-linear decrease with total conversion and EC within the investigated range. The RL agent is

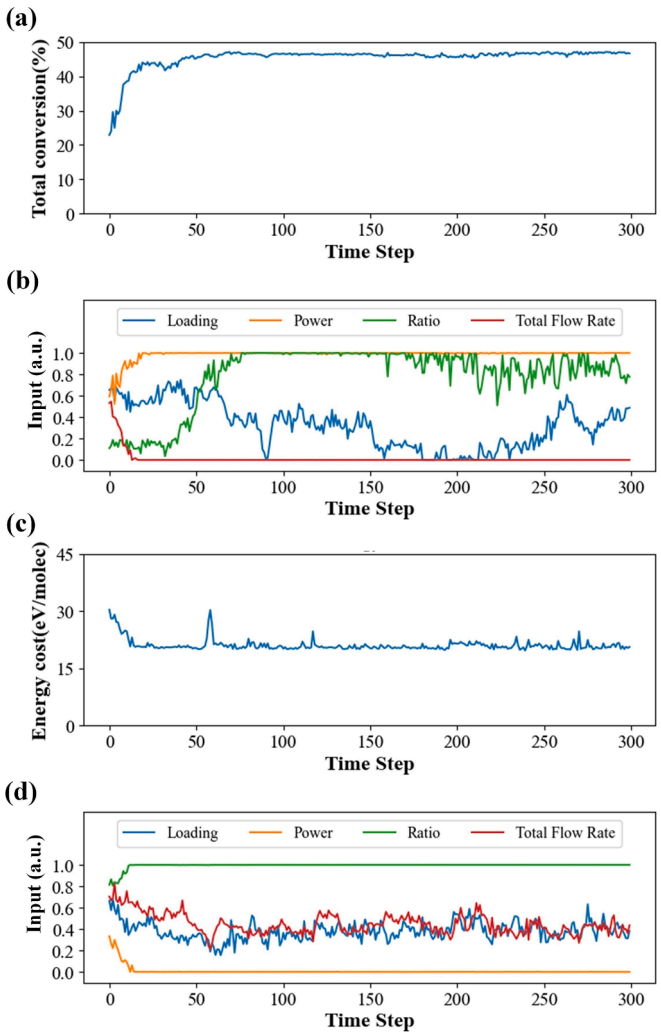

Fig. 7. Testing curve of the RL models of (a) total conversion and (c) energy cost, by plotting them as a function of time step, as well as the corresponding actions (b) and (d), within the investigated range. The y-axis representing the input parameters (for (b) and (d)) shows the normalized values.

trained on the current dataset and learned such near-linear patterns within the investigated range. However, it is not trained by the dataset outside the investigated range. When this very same model is subjected to predictions outside the investigated range, the patterns learned within the investigated range are not effective, which induces an inaccurate RL model. Thus, the agent decreases the negative factor as much as possible, even to a negative value, to obtain the maximum return. This result demonstrates that the RL model can only be effective on patterns prediction and policy optimization within the investigated range.

A similar optimization policy can also be applied to the positive factors. In Fig. 5 and Fig. 6(b and d), the power is the positive factor for the gas conversion and product yield, and the actions of agent are to reach their upper boundary, i.e. at the maximum value of the investigated range. Although the actions of agent are not to reach negative value this time, the maximum value of input parameters depends on the capability of the equipment (e.g. the power supply). Specifically, the RL model might predict that a discharge power of 1 MW is super-efficient for the conversion, but it is impossible to implement. In addition, the safety boundary to implement in experiments should also be considered (e.g. explosion limit when considering $CO_2/CH_4/O_2$ gas mixture for future study). This means that the RL model can only optimize the input parameters within the range of experimental capability.

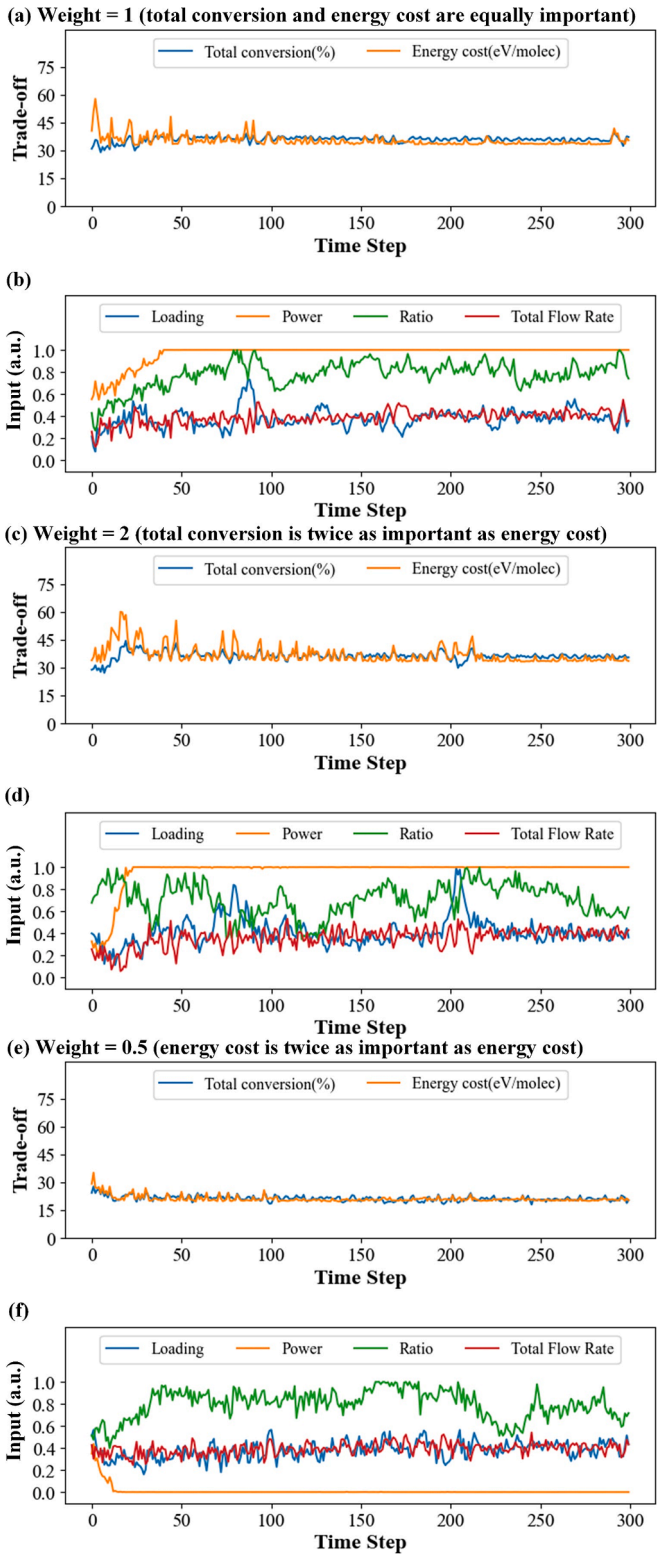

Fig. 8. Superposition of total conversion and energy cost, showing the best trade-offs (a,c,e), as well as the corresponding actions of the four input parameters within the investigated range (b,d,f), for different weights, i.e., weight = 1: (a) and (b), weight = 2: (c) and (d), weight = 0.5: (e) and (f).

4.2. *Optimal policy developed by the RL model*

Comparing the relative significance of the input parameters in Table 2, we can summarize two regulation policies in Table 3: 1) the

Table 3
Regulation sequence of various input parameters within their range.

Objectives	1st order	2nd order	3rd order	4th order
CO_2 conversion ↑	Flow (↓)	Power (↑)	Ratio (↓)	Loading (optimal)
CH_4 conversion ↑	Flow (↓)	Ratio (↑)	Power (↑)	Loading (optimal)
CO yield ↑	Flow (↓)	Ratio (↑)	Power (↑)	Loading (optimal)
H_2 yield ↑	Flow (↓)	Ratio (↑)	Power (↑)	Loading (optimal)
Total conversion ↑	Flow (↓)	Power (↑)	Ratio (optimal); Loading (optimal)	
Energy cost ↓	Power (↓)	Ratio (↑)	Flow (optimal); Loading (optimal)	
Total conversion + energy cost (1 + 1) ↑	Power (↑)	Ratio (optimal)	Flow (near stable) Loading (near stable)	

List of the abbreviations included in the table: Total flow rate (Flow), Discharge power (Power), CO_2 /CH_4 ratio (Ratio) and Ni loading (Loading). When the factors reach their upper and lower bounds, it is represented by (↑) and (↓), respectively. The expected objective is to maximize the reaction performance and minimize the energy cost, which is represented by (↑) and (↓), respectively.

agent's actions on the input parameters are in line with the concluded trend toward the output parameters. To maximize the reaction performance, the positive factors should reach upper bounds and the negative factors should reach lower bounds. When the factors first increase (decrease) and then decrease (increase), they would have an optimal value. To minimize the EC, the power should reach lower bounds and the CO_2/CH_4 ratio should reach upper bounds, since the EC decreases with decreasing power and increasing CO_2/CH_4 ratio. 2) To build the bridge between the agent's actions on the operating parameters and the reaction performance within the investigated range, the optimal sequence can be concluded as follows: the agent ideally starts with a coarse tuning of the more influential parameters, followed by fine-tuning of the less important parameters, to obtain the maximum rewards. In other words, the regulation sequence exhibits good agreement with the predicted significance results. This indicates that the RL agent mimics human experience in the decision-making process. However, the optimization sequence on EC (alone or in combination with total conversion) seems different from the summarized policy, due to the limited training dataset. The most important factor, i.e., total flow rate, which is inversely proportional to energy cost, is not effective, as it is fixed at 75 mL/min in the training dataset near the optimal value for energy cost. If more data could be used for training with different flow rates, the agent can learn a more comprehensive regulation in the current dataset, which is interesting for further investigation.

4.3. Comparison between SL model and RL model

To make a clear comparison between the SL and RL models in terms of performance and application, we list here the advantages and disadvantages of these two approaches:

1) Training efficiency: Training a SL model can be relatively efficient, especially with large datasets and powerful computing resources, while training a RL model is generally less efficient, due to the need for exploration and the potentially long sequences of actions required to learn an optimal policy.
2) Interactivity and adaptability: SL models are generally static, meaning they do not adapt to changes in the environment after training, while RL models are inherently interactive and adaptive, as they learn from the consequences of their actions, so they are well-suited for dynamic environments.

In conclusion, SL models are suitable for tasks that require high precision and accuracy in predictions from static data, while RL models are more appropriate for tasks that involve complex sequences of actions and interactions with a dynamic environment. In many real-world scenarios, a hybrid approach, combining elements of both SL and RL, may offer the best performance and adaptability. Hence, it is interesting to compare the predictions of the SL model (static) with those of the RL model (dynamic) when combining SL and RL models in this work.

To evaluate the RL model's effectiveness, we firstly compare the minimum value of the EC obtained by our RL model with the real experimental dataset, considering that the EC is the most important factor for industrial-scale DRM [45]. According to our RL model, the EC can reach values as low as 21 eV/molec when the discharge power is 20 W and the CO_2/CH_4 ratio is 1.5. This outcome aligns with prior work on the optimal energy yield (EY), which was predicted at same conditions by SL model, and also consistent with the experimental result on EC, reaching 21.3 eV/molec at the same conditions [32].

Similarly, our RL model reveals that the total conversion reaches 36 %, while the EC reaches 34 eV/molec, when the discharge power reaches its upper boundary (i.e. 60 W), the Ni loading is 9.5 wt% and the total flow rate is 74 mL/min. This result is also validated by the experimental dataset on total conversion of 34.0 % and EC of 35.2 eV/molec, at a near same conditions [32]. Therefore, the final results of the actions by the agent and the desired outcome (both maximum total conversion and minimum EC) are in line with the real experimental dataset.

4.4. DBD reactor used for DRM

The Ni loading, the only non-linear factor among these input parameters, has an optimal value at approximately 7.5 % for the performance of plasma-catalytic DRM. This is because the catalyst's specific surface area is larger at lower Ni loading [46], but it can be reduced at higher Ni loading, which in turn diminishes the performance [47], as indicated by studies based on similar preparation method in literature [46,48]. Despite its significant effect, Ni loading is not the dominant factor on the performance, indicated by the relative significance analysis in our work.

Besides Ni loading, the other three factors have much impact on the performance, particularly affecting the reaction kinetics, thermodynamics, and mechanisms, as revealed from literature [7]. As indicated in Figs. 5 to 7, the reaction performance and EC exhibit a near-linear increase with discharge power. In general, higher discharge power leads to more micro-discharges, thereby producing more reaction channels and reactive species, which play an active role in both catalytic surface and gas-phase reactions to boost the CO and H_2 yield [49]. On the contrary, only the EC (alone or in combination with total conversion when the EC weights more than total conversion) hope to reach lower discharge power as the conversion rises less than linearly with rising power, as can be deduced from eq. (3) above [50].

The CO_2/CH_4 ratio positively influences the (absolute) CH_4 conversion and product yield, but it reduces the CO_2 conversion because there are less CH_x radicals that can contribute to the CO_2 conversion, as indicated in Table 2 [50,51]. With higher CO_2 contents, more oxygen atoms generated by CO_2 dissociation can efficiently react with the H atoms produced from CH_4 dissociation through electron impact, thus limiting the backward reaction, $CH_3 + H \rightarrow CH_4$, enabling higher CH_4 conversion [51]. In the meanwhile, the total conversion reaches its maximum for a CO_2/CH_4 ratio of around 1.3. Indeed, the CH_4 conversion is typically higher than the CO_2 conversion (cf. Fig. 5(a) and (c)), suggesting that a CO_2/CH_4 ratio below 1 would be beneficial for the total conversion, but on the other hand, prior works have also demonstrated that CO_2/CH_4 ratios below 1 lead to carbon deposition and catalyst deactivation [52]. By integrating these findings with our model predictions, it is suggested to set a CO_2/CH_4 ratio between 1 and 1.5 for plasma-catalytic DRM applications and it also corresponds with the common composition of biogas [53].

In our work, the EC can reach a minimum value of 12 eV/molec

without any limitation (i.e., when we vary the parameters outside the investigated range) and 21 eV/molec when the parameters are kept within the investigated range. These values are however much higher than the EC target, i.e. 4.3 eV/molecule defined by Snoeckx and Bogaerts [7], to be contentious with traditional DRM, and other promising technologies. The same conclusion about too high energy cost for DBD plasmas was also made in [7], and is generally found in literature (see details in [6]). It should be noted that the task of RL is to aid scientists to optimize the energy cost based on the patterns learned within the investigated range, but they cannot lead to a breakthrough of the physical limitation in DBD reactors. Therefore, we should consider other plasma reactors to enhance the cost-effectiveness of DRM, i.e., warm plasmas like gliding arc, microwave, spark discharge and atmospheric pressure glow discharge (APGD). Indeed, these plasmas can combine energy costs below this target of 4.3 eV/molec with relatively high conversions. For instance, a recent paper from PLASMANT shows that a confined APGD (cAPGD) reactor can reach an EC of 3.5 eV/molec, for a total conversion of 62 % (and at other conditions, an EC of 4.2 eV/molec, for a total conversion of 74 %) [13], while O_2 addition could even reach a lower EC of 1.98 eV/molec for a total conversion of 67 % [54]. These values are clearly lower than the EC target of 4.3 eV/molecule, showing the superior performance of an APGD, and other warm plasmas (yielding similar performance) for DRM. On the other hand, although a DBD reactor cannot reach such excellent performance, it is the most suitable reactor to apply ML, due to the much larger dataset available, because of the much more extensive literature. That is the reason why we applied our ML model to the DBD results. In the future, we also plan to investigate the performance of ML for the other plasma reactor types.

4.5. ML applied to plasma catalysis

ML is crucial in advancing plasma applications that require an accurate description and control of complex plasma-surface interactions, e.g., plasma catalysis [10]. While our data-driven ML model shines at prediction, it cannot explain the fundamental reaction mechanisms, where plasma chemical kinetics models is required, e.g., in Ref. [11] and the specific role of the catalyst for the synergy effect was not considered. Moreover, the results of ML models are mostly validated based on their effectiveness by the experimental dataset and they cannot optimize the reactor performance exceeding its potential [55]. This suggests that the interpretability and potential of ML model can be limited, emphasizing the necessity of prior knowledge in evaluating ML results.

Nevertheless, our ML model demonstrates significant potential for predicting and optimizing other chemical processes, for instance, thermal catalytic DRM. Since catalyst compositions and reactor operation in thermal catalysis have been well-explored through various modeling approaches, our ML methods offer beneficial insights from existing experimental data, achieving enhanced reliability and consistency, to further optimize industrial-scale DRM process.

5. Conclusion

We developed a ML (SL and RL) model to both predict and optimize the plasma-catalytic DRM process, respectively. The SL model utilizes a typical ANN algorithm for reaction performance and cost-effectiveness prediction with a strong connection to the experimental data, indicated by R^2 values close to 1 for all output. However, we go one step further, by also developing a RL model for process optimization. For optimal regulation policy on single output revealed by our RL model, the agent starts with a coarse tuning of the more influential parameters, followed by fine-tuning of the less important parameters. Furthermore, our RL model effectively pinpointed the ideal conditions for achieving the lowest energy cost of 21 eV/molec at lowest bond of discharge power (i.e., 20 W) but highest bond of CO_2/CH_4 ratio (i.e., 1.5), which is in line with our SL prediction and the experimental dataset. For the combined optimization of total conversion and energy cost, our RL model reveals that the discharge power yields a trade-off between both performance metrics. However, an optimal discharge power of 60 W, Ni loading of 9.5 wt% and total flow rate of 74 mL/min resulted in both maximum total conversion and minimum energy cost. Overall, our ML model excels at deriving new insights to facilitate the optimization of intricate nonlinear and dynamic systems, like in plasma-based gas conversion process.

CRediT authorship contribution statement

Jiayin Li: Writing – review & editing, Writing – original draft, Visualization, Methodology, Formal analysis, Data curation, Conceptualization. **Jing Xu:** Writing – review & editing, Writing – original draft, Investigation, Formal analysis. **Evgeny Rebrov:** Writing – review & editing, Writing – original draft. **Annemie Bogaerts:** Writing – review & editing, Supervision, Project administration, Funding acquisition.

Declaration of competing interest

The authors declare that they have no known competing financial interests or personal relationships that could have appeared to influence the work reported in this paper.

Acknowledgments

This project received funding from the European Research Council (ERC) under the European Union's Horizon 2020 research and innovation programme (grant agreement no. 810182-SCOPE ERC Synergy project), and the University of Antwerp BOF-FWO postdoc seal of excellence mandate (grant agreement no. 41/FA070200/FFB240228).

Appendix A. Supplementary data

Supplementary data to this article can be found online at https://doi.org/10.1016/j.cej.2025.159897.

Data availability

Data will be made available on request.

References

[1] D. Pakhare, J. Spivey, A review of dry (CO_2) reforming of methane over noble metal catalysts, Chem. Soc. Rev. 43 (2014) 7813–7837, https://doi.org/10.1039/C3CS60395D.
[2] Y. Kathiraser, U. Oemar, E.T. Saw, Z. Li, S. Kawi, Kinetic and mechanistic aspects for CO_2 reforming of methane over Ni based catalysts, Chem. Eng. J. 278 (2015) 62–78, https://doi.org/10.1016/j.cej.2014.11.143.
[3] H. Zhao, R. Yu, S. Ma, K. Xu, Y. Chen, K. Jiang, Y. Fang, C. Zhu, X. Liu, Y. Tang, L. Wu, Y. Wu, Q. Jiang, P. He, Z. Liu, L. Tan, The role of Cu1–O_3 species in single-atom Cu/ZrO_2 catalyst for CO_2 hydrogenation, Nat. Catal. 5 (2022) 818–831, https://doi.org/10.1038/s41929-022-00840-0.
[4] Y. Song, E. Ozdemir, S. Ramesh, A. Adishev, S. Subramanian, A. Harale, M. Albuali, B.A. Fadhel, A. Jamal, D. Moon, S.H. Choi, C.T. Yavuz, Dry reforming of methane by stable Ni–Mo nanocatalysts on single-crystalline MgO, Science 367 (2020) 777–781, https://doi.org/10.1126/science.aav2412.
[5] W. Lu, Q. Cao, B. Xu, H. Adidharma, K. Gasem, M. Argyle, F. Zhang, Y. Zhang, M. Fan, A new approach of reduction of carbon dioxide emission and optimal use of carbon and hydrogen content for the desired syngas production from coal, J. Clean. Prod. 265 (2020) 121786, https://doi.org/10.1016/j.jclepro.2020.121786.
[6] A. George, B. Shen, M. Craven, Y. Wang, D. Kang, C. Wu, X. Tu, A review of non-thermal plasma technology: a novel solution for CO_2 conversion and utilization, Renew. Sustain. Energy Rev. 135 (2021) 109702, https://doi.org/10.1016/j.rser.2020.109702.
[7] R. Snoeckx, A. Bogaerts, Plasma technology – a novel solution for CO_2 conversion? Chem. Soc. Rev. 46 (2017) 5805–5863, https://doi.org/10.1039/C6CS00066E.
[8] D.B. Nguyen, S. Saud, Q.T. Trinh, H. An, N.-T. Nguyen, Q.H. Trinh, H.T. Do, Y. S. Mok, W.G. Lee, Generation of multiple jet capillaries in advanced dielectric barrier discharge for large-scale plasma jets, Plasma Chem. Plasma P. 43 (2023) 1475–1488, https://doi.org/10.1007/s11090-023-10404-0.
[9] J. Osorio-Tejada, M. Escriba-Gelonch, R. Vertongen, A. Bogaerts, V. Hessel, CO_2 conversion to CO via plasma and electrolysis: a techno-economic and energy cost

analysis, Energy Environ. Sci. 17 (2024) 5833–5853, https://doi.org/10.1039/D4EE00164H.
[10] A. Bogaerts, X. Tu, J.C. Whitehead, G. Centi, L. Lefferts, O. Guaitella, F. Azzolina-Jury, H.-H. Kim, A.B. Murphy, W.F. Schneider, T. Nozaki, J.C. Hicks, A. Rousseau, F. Thevenet, A. Khacef, M. Carreon, The 2020 plasma catalysis roadmap, J. Phys. D: Appl. Phys. 53 (2020) 443001, https://doi.org/10.1088/1361-6463/ab9048.
[11] B. Loenders, R. Michiels, A. Bogaerts, Is a catalyst always beneficial in plasma catalysis? Insights from the many physical and chemical interactions, J. Energy Chem. 85 (2023) 501–533, https://doi.org/10.1016/j.jechem.2023.06.016.
[12] A. Bogaerts, E.C. Neyts, Plasma technology: an emerging technology for energy storage, ACS Energy Lett. 3 (2018) 1013–1027, https://doi.org/10.1021/acsenergylett.8b00184.
[13] B. Wanten, S. Maerivoet, C. Vantomme, J. Slaets, G. Trenchev, A. Bogaerts, Dry reforming of methane in an atmospheric pressure glow discharge: confining the plasma to expand the performance, J. CO_2 Util. 56 (2022) 101869, https://doi.org/10.1016/j.jcou.2021.101869.
[14] A. Azizinia, H.R. Bozorgzadeh, N. Seyed-Matin, M. Baghalha, A. Mohamadalizadeh, Comparison of dry reforming of methane in low temperature hybrid plasma-catalytic corona with thermal catalytic reactor over Ni/γ-Al_2O_3, J. Nat. Gas Chem. 21 (2012) 466–475, https://doi.org/10.1016/S1003-9953(11)60392-7.
[15] J. Martin-del-Campo, M. Uceda, S. Coulombe, J. Kopyscinski, Plasma-catalytic dry reforming of methane over Ni-supported catalysts in a rotating gliding arc – Spouted bed reactor, J. CO_2 Util. 46 (2021) 101474, https://doi.org/10.1016/j.jcou.2021.101474.
[16] O. Biondo, C.F.A.M. van Deursen, A. Hughes, A. van de Steeg, W. Bongers, M.C. M. van de Sanden, G. van Rooij, A. Bogaerts, Avoiding solid carbon deposition in plasma-based dry reforming of methane, Green Chem. 25 (2023) 10485–10497, https://doi.org/10.1039/D3GC03595F.
[17] S. Li, J. Sun, Y. Gorbanev, K. van't Veer, B. Loenders, Y. Yi, T. Kenis, Q. Chen, A. Bogaerts, Plasma-assisted dry reforming of CH_4: how small amounts of O_2 addition can drastically enhance the oxygenate production–experiments and insights from plasma chemical kinetics modeling, ACS Sustain. Chem. Eng. 11 (2023) 15373–15384, https://doi.org/10.1021/acssuschemeng.3c04352.
[18] M. Ronda-Lloret, Y. Wang, P. Oulego, G. Rothenberg, X. Tu, N.R. Shiju, CO_2 hydrogenation at atmospheric pressure and low temperature using plasma-enhanced catalysis over supported cobalt oxide catalysts, ACS Sustainable Chem. Eng. 8 (2020) 17397–17407, https://doi.org/10.1021/acssuschemeng.0c05565.
[19] B. Ashford, Y. Wang, C.-K. Poh, L. Chen, X. Tu, Plasma-catalytic conversion of CO_2 to CO over binary metal oxide catalysts at low temperatures, Appl. Catal. B Environ. 276 (2020) 119110, https://doi.org/10.1016/j.apcatb.2020.119110.
[20] D. Mei, B. Ashford, Y.-L. He, X. Tu, Plasma-catalytic reforming of biogas over supported Ni catalysts in a dielectric barrier discharge reactor: effect of catalyst supports, Plasma Process. Polym. 14 (2017) 1600076, https://doi.org/10.1002/ppap.201600076.
[21] N. Lu, D. Sun, Y. Xia, K. Shang, B. Wang, N. Jiang, J. Li, Y. Wu, Dry reforming of CH_4CO_2 in AC rotating gliding arc discharge: effect of electrode structure and gas parameters, Int. J. Hydrogen Energy 43 (2018) 13098–13109, https://doi.org/10.1016/j.ijhydene.2018.05.053.
[22] R.S. Abiev, D.A. Sladkovskiy, K.V. Semikin, D.Y. Murzin, E.V. Rebrov, Non-thermal plasma for process and energy intensification in dry reforming of methane, Catalysts 10 (2020) 1358, https://doi.org/10.3390/catal10111358.
[23] M. Witman, D. Gidon, D.B. Graves, B. Smit, A. Mesbah, Sim-to-real transfer reinforcement learning for control of thermal effects of an atmospheric pressure plasma jet, Plasma Sources Sci. Technol. 28 (2019) 095019, https://doi.org/10.1088/1361-6595/ab3c15.
[24] A.D. Bonzanini, K. Shao, D.B. Graves, S. Hamaguchi, A. Mesbah, Foundations of machine learning for low-temperature plasmas: methods and case studies, Plasma Sources Sci. Technol. 32 (2023) 024003, https://doi.org/10.1088/1361-6595/acb28c.
[25] U.K. Ercan, G.D. Özdemir, M.A. Özdemir, O. Güren, Plasma medicine: the era of artificial intelligence, Plasma Process. Polym. 20 (2023) e2300066, https://doi.org/10.1002/ppap.202300066.
[26] M. Suvarna, T.P. Araújo, J. Pérez-Ramírez, A generalized machine learning framework to predict the space-time yield of methanol from thermocatalytic CO_2 hydrogenation, Appl. Catal. B Environ. 315 (2022) 121530, https://doi.org/10.1016/j.apcatb.2022.121530.
[27] A. Bhardwaj, A.S. Ahluwalia, K.K. Pant, S. Upadhyayula, A principal component analysis assisted machine learning modeling and validation of methanol formation over Cu-based catalysts in direct CO_2 hydrogenation, Sep. Purif. Technol. 324 (2023) 124576, https://doi.org/10.1016/j.seppur.2023.124576.
[28] Y. Wang, Z. Liao, S. Mathieu, F. Bin, X. Tu, Prediction and evaluation of plasma arc reforming of naphthalene using a hybrid machine learning model, J. Hazard. Mater. 404 (2021) 123965, https://doi.org/10.1016/j.jhazmat.2020.123965.
[29] S.Y. Liu, D.H. Mei, Z. Shen, X. Tu, Nonoxidative conversion of methane in a dielectric barrier discharge reactor: prediction of reaction performance based on neural network model, J. Phys. Chem. C 118 (2014) 10686–10693, https://doi.org/10.1021/jp502557s.
[30] X. Zhu, S. Liu, Y. Cai, X. Gao, J. Zhou, C. Zheng, X. Tu, Post-plasma catalytic removal of methanol over Mn–Ce catalysts in an atmospheric dielectric barrier discharge, Appl. Catal. B Environ. 183 (2016) 124–132, https://doi.org/10.1016/j.apcatb.2015.10.013.
[31] Y. Wang, Y. Chen, J. Harding, H. He, A. Bogaerts, X. Tu, Catalyst-free single-step plasma reforming of CH_4 and CO_2 to higher value oxygenates under ambient conditions, Chem. Eng. J. 450 (2022) 137860, https://doi.org/10.1016/j.cej.2022.137860.
[32] Y. Cai, D. Mei, Y. Chen, A. Bogaerts, X. Tu, Machine learning-driven optimization of plasma-catalytic dry reforming of methane, J. Energy Chem. 96 (2024) 153–163, https://doi.org/10.1016/j.jechem.2024.04.022.
[33] A. Mesbah, D.B. Graves, Machine learning for modeling, diagnostics, and control of non-equilibrium plasmas, J. Phys. D: Appl. Phys. 52 (2019) 30LT02, https://doi.org/10.1088/1361-6463/ab1f3f.
[34] R.S. Sutton, A.G. Barto, Reinforcement Learning: An Introduction, MIT Press, Cambridge, MA, USA, 2018.
[35] Z. Hou, T. Lee, M. Keidar, Reinforcement learning with safe exploration for adaptive plasma cancer treatment, IEEE Trans. Radiat. Plasma Med. Sci. 6 (2022) 482–492, https://doi.org/10.1109/TRPMS.2021.3094874.
[36] B. Wanten, R. Vertongen, R.D. Meyer, A. Bogaerts, Plasma-based CO_2 conversion: how to correctly analyze the performance? J. Energy Chem. 86 (2023) 180, https://doi.org/10.1016/j.jechem.2023.07.005.
[37] T. Nishida, Data transformation and normalization, Rinsho Byori 58 (2010) 990–997.
[38] X. Wang, X. Du, K. Chen, Z. Zheng, Y. Liu, X. Shen, C. Hu, Predicting the ammonia synthesis performance of plasma catalysis using an artificial neural network model, ACS Sustainable Chem. Eng. 11 (2023) 4543–4554, https://doi.org/10.1021/acssuschemeng.2c04715.
[39] J. Li, L. Pan, M. Suvarna, X. Wang, Machine learning aided supercritical water gasification for H_2-rich syngas production with process optimization and catalyst screening, Chem. Eng. J. 426 (2021) 131285, https://doi.org/10.1016/j.cej.2021.131285.
[40] Y. Shen, C. Fu, W. Luo, Z. Liang, Z.-R. Wang, Q. Huang, Machine learning for CO_2 conversion driven by dielectric barrier discharge plasma and Cs_2TeC_{l6} photocatalysts, Green Chem. 25 (2023) 7605–7611, https://doi.org/10.1039/D3GC02354K.
[41] D. Tan, M. Suvarna, Y. Shee Tan, J. Li, X. Wang, A three-step machine learning framework for energy profiling, activity state prediction and production estimation in smart process manufacturing, Appl. Energy 291 (2021) 116808, https://doi.org/10.1016/j.apenergy.2021.116808.
[42] X. Yuan, M. Suvarna, S. Low, P.D. Dissanayake, K.B. Lee, J. Li, X. Wang, Y.S. Ok, Applied machine learning for prediction of CO_2 adsorption on biomass waste-derived porous carbons, Environ. Sci. Technol. 55 (2021) 11925–11936, https://doi.org/10.1021/acs.est.1c01849.
[43] Y. Gao, Z. Saedi, H. Shi, B. Zeng, B. Zhang, X. Zhang, Machine learning-assisted optimization of microbubble-enhanced cold plasma activation for water treatment, ACS EST Water 4 (2024) 735–750, https://doi.org/10.1021/acsestwater.3c00783.
[44] J. Schulman, F. Wolski, P. Dhariwal, A. Radford, O. Klimov, Proximal Policy Optimization Algorithms, (2017). https://doi.org/10.48550/arXiv.1707.06347.
[45] A.H. Khoja, A. Mazhar, F. Saleem, M.T. Mehran, S.R. Naqvi, M. Anwar, S. Shakir, N.A. Saidina Amin, M.B. Sajid, Recent developments in catalyst synthesis using DBD plasma for reforming applications, Int. J. Hydrogen Energy 46 (2021) 15367–15388, https://doi.org/10.1016/j.ijhydene.2021.02.043.
[46] Sk. Mahammadunnisa, P. Manoj Kumar Reddy, B. Ramaraju, Ch. Subrahmanyam, Catalytic nonthermal plasma reactor for dry reforming of methane, Energy Fuels 27 (2013) 4441–4447, https://doi.org/10.1021/ef302193e.
[47] N. Sahli, C. Petit, A.C. Roger, A. Kiennemann, S. Libs, M.M. Bettahar, Ni catalysts from $NiAl_2O_4$ spinel for CO_2 reforming of methane, Catal. Today 113 (2006) 187–193, https://doi.org/10.1016/j.cattod.2005.11.065.
[48] Q. Wang, B.-H. Yan, Y. Jin, Y. Cheng, Dry reforming of methane in a dielectric barrier discharge reactor with Ni/Al_2O_3 catalyst: interaction of catalyst and plasma, Energy Fuels 23 (2009) 4196–4201, https://doi.org/10.1021/ef900286j.
[49] A. Bogaerts, T. Kozák, K. van Laer, R. Snoeckx, Plasma-based conversion of CO_2: current status and future challenges, Faraday Discuss. 183 (2015) 217–232, https://doi.org/10.1039/C5FD00053J.
[50] R. Snoeckx, Y.X. Zeng, X. Tu, A. Bogaerts, Plasma-based dry reforming: improving the conversion and energy efficiency in a dielectric barrier discharge, RSC Adv. 5 (2015) 29799–29808, https://doi.org/10.1039/C5RA01100K.
[51] R. Snoeckx, R. Aerts, X. Tu, A. Bogaerts, Plasma-based dry reforming: a computational study ranging from the nanoseconds to seconds time scale, J. Phys. Chem. C 117 (2013) 4957–4970, https://doi.org/10.1021/jp311912b.
[52] J.-M. Lavoie, Review on dry reforming of methane, a potentially more environmentally-friendly approach to the increasing natural gas exploitation, Front. Chem. 2 (2014), https://doi.org/10.3389/fchem.2014.00081.
[53] D. Mei, X. Shen, S. Liu, R. Zhou, X. Yuan, Z. Rao, Y. Sun, Z. Fang, X. Du, Y. Zhou, X. Tu, Plasma-catalytic reforming of biogas into syngas over Ni-based bimetallic catalysts, Chem. Eng. J. 462 (2023) 142044, https://doi.org/10.1016/j.cej.2023.142044.
[54] S. Maerivoet, B. Wanten, R. De Meyer, M. Van Hove, S. Van Alphen, A. Bogaerts, Effect of O_2 on plasma-based dry reforming of methane: revealing the optimal gas composition via experiments and modeling of an atmospheric pressure glow discharge, ACS Sustainable Chem. Eng. (2024), https://doi.org/10.1021/acssuschemeng.4c04283.
[55] T. Toyao, Z. Maeno, S. Takakusagi, T. Kamachi, I. Takigawa, K. Shimizu, Machine learning for catalysis informatics: recent applications and prospects, ACS Catal. 10 (2020) 2260–2297, https://doi.org/10.1021/acscatal.9b04186.